Chemistry Europe
European Chemical Societies Publishing

WILEY VCH

Excellence in Chemistry Research

Announcing our new flagship journal

- Gold Open Access
- Publishing charges waived
- Preprints welcome
- Edited by active scientists

Meet the Editors of *ChemistryEurope*

Luisa De Cola
Università degli Studi di Milano Statale, Italy

Ive Hermans
University of Wisconsin-Madison, USA

Ken Tanaka
Tokyo Institute of Technology, Japan

ChemistrySelect

Research Article
doi.org/10.1002/slct.202301263

Chemistry Europe
European Chemical Societies Publishing

www.chemistryselect.org

Effect of Different Amounts of Pt on Fe_3O_4–TiO_2 for Photocatalytic H_2 Production Under Solar Light

Irem Firtina-Ertis*[a] and Özge Kerkez-Kuyumcu[b]

In this study, Pt doped Fe_3O_4–TiO_2 photocatalysts were synthesized in two steps; (i) Fe_3O_4–TiO_2 (FT) was prepared by the complex-assisted vapor thermal (VT) method, (ii) Pt was doped to Fe_3O_4–TiO_2 (FT–Pt) by the polyol method. The effect of different amounts of Pt was investigated for photocatalytic hydrogen production. The absorption spectrum of FT with 5.0% Pt exhibits a surface plasmon resonance (SPR) peak of ~420 nm which corresponds to the band gap of 2.95 eV. The FT and Pt doped FT samples showed a less intense photoluminescence (PL) band than TiO_2 (T) due to the lower e^-/h^+ recombination rate. By increasing %wt. Pt in the FT samples, PL intensity was decreased. Thus, Pt plays an essential role to hinder the recombination of e^-/h^+ pairs. Consequently, FT-5.0% Pt showed 144 μmol/g-cat H_2 production rate, just about 3.3 times higher than that of FT photocatalyst; due to the suitable band gap energy and the retarded e^-/h^+ recombination. Therefore, the synergistic effect of Pt and Fe_3O_4 is found to be beneficial to decrease the e^-/h^+ recombination rate thus the photocatalytic activity enhancement was achieved.

Introduction

Photocatalytic hydrogen production is a promising method in the usage of renewable energy sources. TiO_2 is crucial as a semiconductor in photocatalytic applications because of its durability, non-toxicity, high oxidizing power, etc.[1] However, TiO_2 has two important shortcomings that limit its photocatalytic activity. The first shortcoming of TiO_2 is photoactivation by only UV light attributed to the wavelength of 390 nm due to its wide bandgap. For TiO_2 to support solar light as a photocatalyst, it needs band gap modification because solar light contains a small fraction of UV light and besides 42–47% visible light.[2–3] Thus, the band gap energy of TiO_2 should be adjusted to increase response to solar light. The other shortcoming is about recombination of photo-excited electron/hole (e^-/h^+) pairs. The photocatalytic reaction initiates with the light absorption corresponding to the band gap energy of TiO_2, and electron-hole (e^-/h^+) pairs are formed ($TiO_2 + hv \rightarrow e^-(CB) + h^+(VB)$). Recombination of these photo-excited e^-/h^+ pairs cause low photocatalytic activity.[4] Therefore, TiO_2 needs some additives to alter the band gap energy and to retard the e^-/h^+ recombination rate.[5] There are numerous studies about modifying TiO_2 to obtain suitable band gap and retarded e^-/h^+ recombination.[6–11] Metals like Ce, Fe, etc., metal oxides like $CuCr_2O_4$, WO_x, etc., and anions like N, B, and C have been used in the modification of TiO_2.[8,12–14] Also, modification of TiO_2 with noble metals such as Pt, Au, Pd, and Ag ensures trapping charge carriers thus decreasing the e^-/h^+ recombination rate.[4]

As distinct from these insufficiencies of TiO_2, another hot topic is the effortless separation of the photocatalyst from the reaction medium. Recently, in photocatalytic applications especially in photocatalytic organic substance degradation, Fe_3O_4 (magnetite)-TiO_2 usage has emerged due to the ease of magnetic separation.[15] g-C_3N_4/Fe_3O_4/TiO_2 was used in the degradation of both dinitro butyl phenol and methylene blue under visible light irradiation;[16] Fe_3O_4-mesoporous TiO_2/C was used in the degradation of bisphenol A under visible light;[17] Fe_3O_4–TiO_2/RGO was used in the degradation of phenol under 365 nm;[18] Fe_3O_4/TiO_2/$CoMoO_4$ was used in the degradation of organic dyes under sunlight irradiation;[19] Fe_3O_4@SiO_2@g-C_3N_4/TiO_2 core-shell microsphere structured photocatalyst was used in Rhodamine B and Methyl Orange degradation under visible light;[20] Fe_3O_4@TiO_2 heterojunction photocatalysts were used to remove Bisphenol A (BPA) under visible and long wavelength UV light irradiation;[21] TiO_2/Fe_3O_4 was used for decomposition of metronidazole.[22] Besides, the synergistic effect of noble metal and Fe_3O_4 on TiO_2 found as worth investigating in terms of photocatalytic activity enhancement. For example, Fe_3O_4@TiO_2–Au, Fe_3O_4/TiO_2/Ag, and Fe_3O_4@Ru-doped TiO_2 as trio concept photocatalysts were used in similar photocatalytic degradation experiments.[23–26]

To the best of our knowledge, there are a few reports for photocatalytic H_2 production by using Fe_3O_4–TiO_2 photocatalysts. For example, nano-fibrillated cellulose/magnetite/titanium dioxide (NFC@Fe_3O_4@TNP) nanocomposites were used for photocatalytic H_2 production under UV light.[27] In another study, Ag plasmons-sensitized magnetic-Fe_3O_4 integrated TiO_2 (Ag–Fe_3O_4@TiO_2) ternary nanocomposites were used for both dye degradation and H_2 generation under light and dark conditions. They observed red shift along with a distinct

[a] Dr. I. Firtina-Ertis
Gebze Technical University, Faculty of Engineering
Chemical Engineering Department
Gebze, Kocaeli, 41400, Turkey
E-mail: iremertis@gtu.edu.tr

[b] Dr. Ö. Kerkez-Kuyumcu
Marmara University, Faculty of Engineering
Chemical Engineering Department
Maltepe, İstanbul, 34854, Turkey

Supporting information for this article is available on the WWW under https://doi.org/10.1002/slct.202301263

plasmonic band in the UV-visible absorption spectrum due to metallic Ag nanoparticles, which was confirmed by the PL spectrum with an effective electron and hole separation.[28] Furthermore, mono- and co-doped TiO_2 (Co^{n+} and Fe^{n+}) were prepared by sol-gel technique under solar light. They have found the existence of multivalent states of Fe and Co ions together improved solar light absorption of TiO_2, inhibited the recombination of photogenerated charges, and consequently enhanced the photocatalytic efficiency.[29]

This work proposes the usage of a trio concept solar-light driven photocatalyst Pt doped Fe_3O_4–TiO_2 in hydrogen production; thus, it has three goals which are modification of band gap to support the solar light, retarded e^-/h^+ recombination, easy separation of the photocatalyst. Pt doped Fe_3O_4–TiO_2 photocatalysts were synthesized via two steps: (i) Fe_3O_4–TiO_2 was prepared by a complex assisted vapor thermal (VT) method reported in our previous study,[30] (ii) Pt was doped to Fe_3O_4–TiO_2 by the polyol method. This is the first time that these two methods were used sequentially. Different %wt. amounts of Pt in the photocatalyst were investigated in terms of hydrogen production rate.

Results and Discussion

Characterization Results

The structure and the average crystallite size of the photocatalysts were analyzed by X-ray powder diffraction (XRD). Figure 1 shows the XRD peaks for the prepared Fe_3O_4 (F), TiO_2 (T), and Fe_3O_4–TiO_2 (FT) photocatalysts with different %wt. of Pt (%wt. 0, 0.5, 1, 2.5, and 5). The XRD peaks of the anatase structure of TiO_2 were monitored at $2\theta = 25.24°$, 37.08°, 37.91°, 38.65°, 48.10°, 53.97°, 55.07°, and 62.87° attributed to the (101), (103), (004), (112), (200), (105), (211) and (204) planes, respectively (JCPDS No. 21-1272).[31] While the Fe_3O_4 (magnetite) diffraction peaks with cubic spinel structure appearing at $2\theta =$ 30.2°, 35.6°, 43.3°, 53.5°, 57.44°, and 63° can be attributed to the (2 0 0), (3 1 1), (4 0 0), (4 2 2), (5 1 1) and (440) lattice plane of Fe_3O_4 (JCPDS Card No. 89-3854), respectively.[21–22]

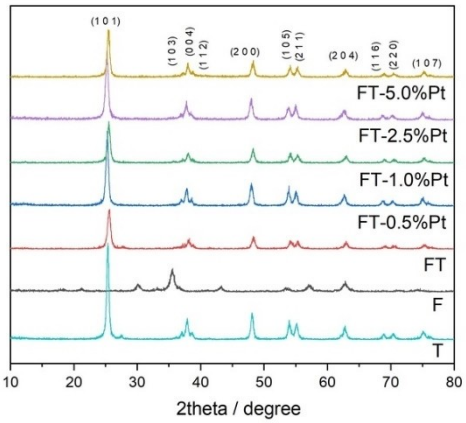

Figure 1. XRD diffraction peaks of Fe_3O_4 (F), TiO_2(T), and Fe_3O_4–TiO_2 (FT) photocatalysts with different %wt of Pt (%wt 0, 0.5, 1, 2.5, and 5).

Fe_3O_4 is only used to provide magnetic properties to the catalyst because the higher amount of Fe_3O_4 is not favorable for photocatalytic applications in terms of causing a higher e^-/h^+ recombination rate.[32] In a study from the literature, they used different ratios for Fe_3O_4–TiO_2. However, they have found that the photocatalytic activity of the photocatalyst in dye degradation reaction decreases with increasing the amount of Fe_3O_4 in the photocatalyst (Fe_3O_4–TiO_2).[33] Another study used Fe_3O_4@TiO_2-P25 composite which was established as a type-I heterojunction photocatalyst according to the energy band set-up values. In this type of photocatalyst, the photogenerated carriers would transfer across the heterojunction interface and accumulate on the Fe_3O_4 semiconductor and may act as an electron-hole recombination center.[34] Madima et al. have prepared Fe_3O_4–TiO_2 photocatalysts with different amounts of (%wt. 5, 10, 20, 30, 50, 70) Fe_3O_4 and they have found similar photoluminescence intensity.[35] Therefore, we have only studied with a constant amount of Fe_3O_4(% 4 wt.) and investigated the %wt. different amounts of Pt.

For the FT samples, all the diffraction peaks could be indexed to the anatase phases of TiO_2 due to the low %wt. of Fe_3O_4. In addition, it is easy to observe that the main characteristic peaks did not noticeably change during the synthesis of FT regardless of the %wt. amount of Pt doping. No reflections regarding Pt were observed due to the low wt.% of Pt without forming oxides on the FT surface.[26] There is no peak from the impurity phase in FT photocatalysts. The presence of Pt has been verified by the TEM elemental analysis.

The average crystallite size of Fe_3O_4 (F), TiO_2 (T), and Fe_3O_4–TiO_2 (FT) photocatalysts with different %wt. of Pt (%wt. 0, 0.5, 1, 2.5, and 5) ranged between 13.7 and 16.4 nm (Table 1). The average crystallite size from the XRD peak at $2\theta = 25.24°$ was calculated by the Debye-Scherrer equation as seen below.[15]

$$D = \frac{k\lambda}{\beta cos\theta} \quad (1)$$

where D is the crystallite size (nm), λ is the X-ray wavelength (nm), k is a constant related to the crystallite shape and taken as 0.9, β is the peak width at half maximum (FWHM) of the XRD peak and θ is the diffraction angle.[36]

The intensity of the peak at $2\theta = 25.24°$ of the FT photocatalyst was decreased and broadened with respect to that of bare TiO_2 whereas Pt doping to FT caused the increased peak

Table 1. Crystallite size and Band gap energies of the photocatalysts.

Photocatalyst	D (nm)	Band gap Energy (eV)
TiO_2 (T)	17.8	3.28
FT	13.7	3.25
FT-0.5% Pt	15.6	3.19
FT-1.0% Pt	15.4	3.16
FT-2.5% Pt	14.3	3.05
FT-5.0% Pt	16.4	2.95

intensity and narrower peak again, which shows higher crystallite size as seen in Table 1.

TEM images and elemental mapping were used to investigate its microstructure, morphology and identify the elements, respectively. Figure 2 shows the elemental mapping of the FT-5.0% Pt photocatalyst. Fe_3O_4 and TiO_2 nanoparticles are homogeneously distributed with a diameter below 20 nm. Pt (in blue color) in the photocatalyst can be observed easily.

Figure 3 (a) shows the UV-vis absorbance spectra of single TiO_2 (T), FT, and FT with different wt.% of Pt (%wt. 0, 0.5, 1, 2.5, and 5). The bare TiO_2 shows the absorption band edge between 350 and 380 nm, indicating a bandgap of 3.2 eV[15] and the absorption peak is 500 nm for Fe_3O_4 corresponding to a narrow band gap of ~2.2 eV.[26] The absorption band edges of the FT photocatalysts with Pt exhibited a remarkably red-shift (means increasing in wavelength) which can be explained by the surface-plasmon-resonance (SPR) effect of TiO_2 and Pt[37] and extended to the visible light region whereas FT has nearly the same peak as TiO_2.[38] Pt impurity level is beneficial for extending the absorption spectrum wavelength towards the visible region. The powerful absorption of Pt due to the surface plasmon resonance (SPR) can form a good absorption in the visible light region.[39]

In Figure 3 (a), the absorption spectrum of FT with 5.0% Pt exhibits a SPR peak of ~420 nm which corresponds to the band gap of 2.95 eV. Increasing the amount of %wt. Pt in the photocatalyst has a positive impact on the absorbance spectrum in the visible region arising from the faster charge transfer between Pt and TiO_2, the increased synergistic effect via Pt doping to FT, and the reduced band gap energy of the

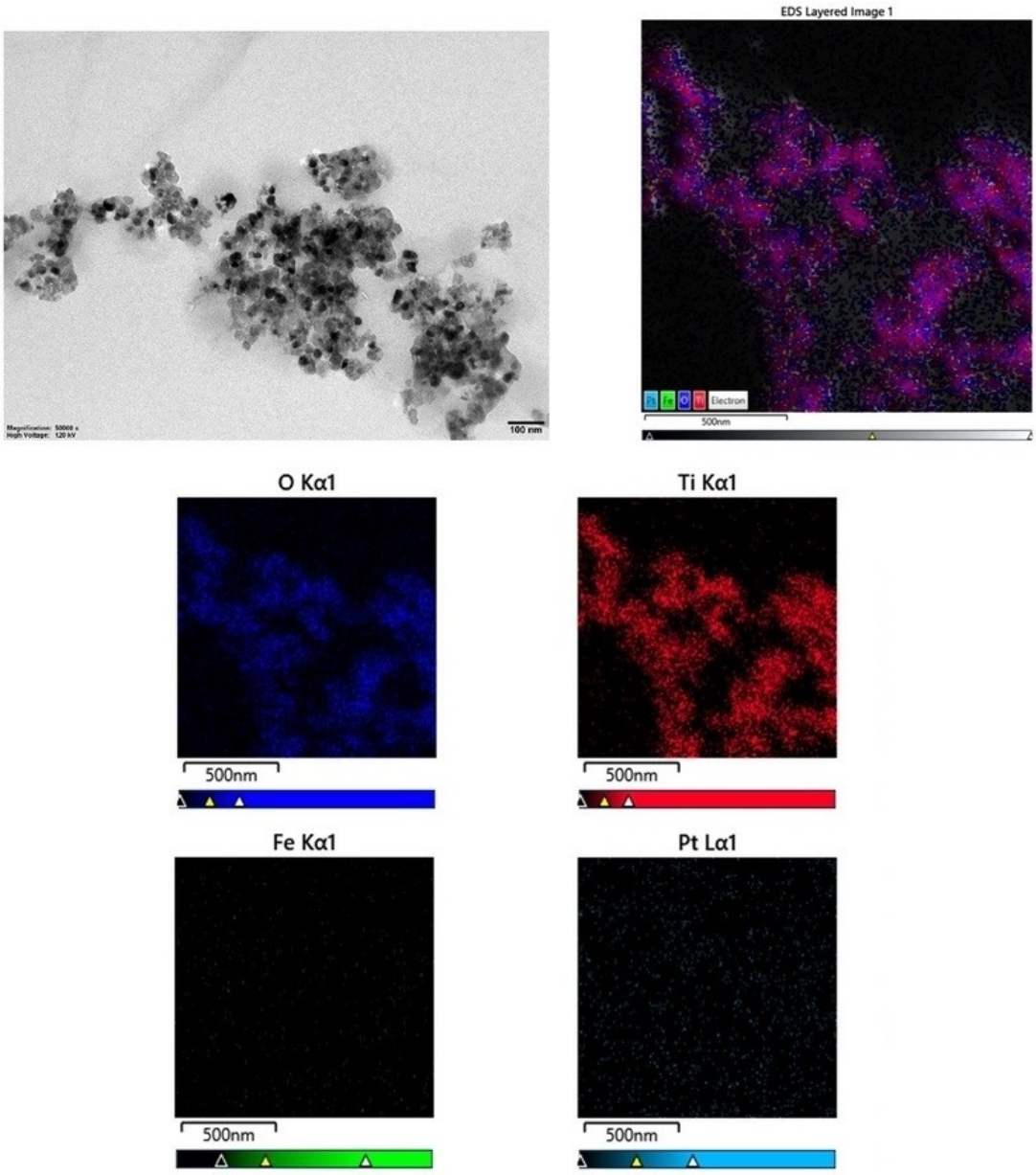

Figure 2. TEM image and elemental mapping of FT-5.0% Pt photocatalyst.

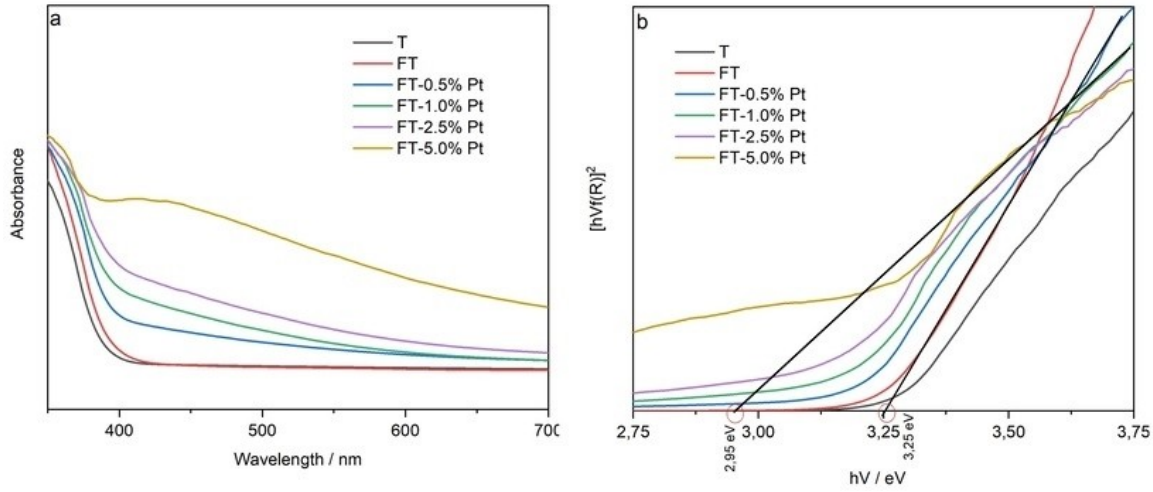

Figure 3. (a) UV-vis absorbance spectrum and (b) Tauc plots of TiO2 (T), FT with different wt.% of Pt (% wt 0, 0.5, 1, 2.5, and 5).

photocatalyst.[26] The increased response to the visible light absorption of Pt doped FT is attributed to the low energy transitions between the energy levels of Pt and TiO_2. Thus, the FT photocatalyst showed a bandgap of 3.25 eV whereas the FT-5.0% Pt photocatalyst had 2.95 eV bandgap energy.

The curve of photon energy (hν) versus $[h\nu f(R)]^2$ called as Tauc plot was used to pinpoint the bandgap energy of the photocatalysts.[40–41] In most of the articles, the Fe_3O_4–TiO_2 photocatalysts have been treated as direct band gap which depends on the nature of transition (n = 2 for direct band gap).[42–43] Thus, we assumed that our photocatalysts are direct band gap semiconductors.

Figure 3(b) shows the Tauc plots of bare TiO_2 (T), FT, and FT with different wt.% of Pt. The band gap energies were determined using Tauc plots in Figure 3(b) by extrapolating the linear region of the plot to the intercept of the photon energy axis in Figure 3(a). The direct bandgap energy of the samples was evaluated from Tauc plots by:

$$(\alpha h\nu)^n = A(h\nu - E_g) \quad (2)$$

where E_g is the band gap energy, h is Planck's constant, ν is the frequency of vibration, hν is the photon energy, A is a proportional constant and α is the absorption coefficient. The Kubelka-Munk function of the reflectance (f(R)) is proportional to the absorption coefficient, α.[44–45] The direct allowed transition (n = 2) is used for all samples. Bandgap energy of the single TiO_2, FT, FT-0.5% Pt, FT-1.0% Pt, FT-2.5% Pt and FT-5.0% Pt photocatalysts were demonstrated in Table 1 as 3.28 eV, 3.25 eV, 3.19 eV, 3.16 eV, 3.05 eV, and 2.95 eV, respectively.

In photoluminescence spectroscopy, firstly the defective regions were identified by Gaussian deconvolution of PL spectrum of bare TiO_2. Four Gaussian peaks (P1-P4) were identified centered at 496 nm, 541 nm, 621 nm, and 649 nm, as seen in Figure 4(a), which are attributed to three different physical situations such as self-trapped excitons, oxygen vacancies, and surface states.[46] The peaks centered at 496 nm

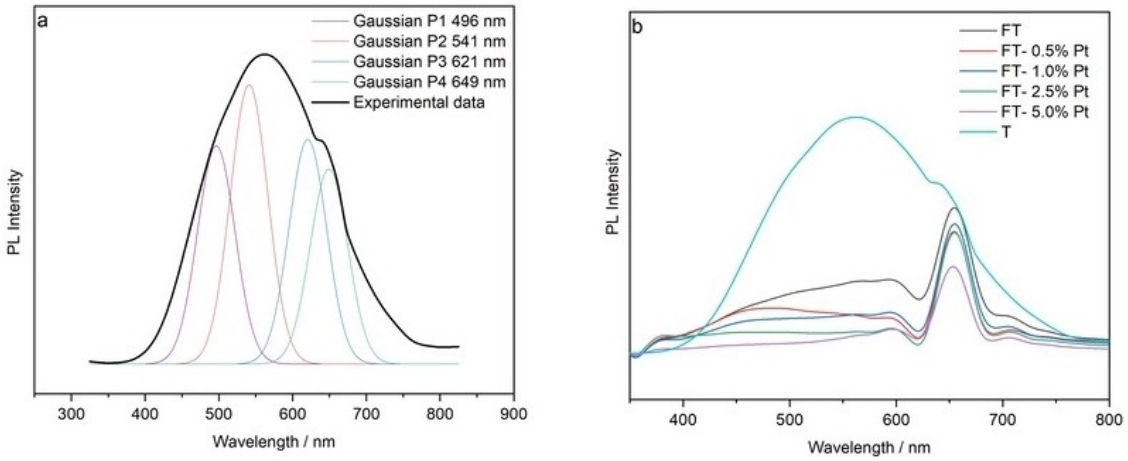

Figure 4. Photoluminescence (PL) spectrum of (a) deconvoluted Gaussian peaks of TiO2 (b) Fe2O3–TiO2 (FT) photocatalysts with different % wt of Pt (% wt 0, 0.5, 1, 2.5, and 5).

and 621 nm were detected in the photoluminescence spectrum of the TiO_2 because of back-stimulation of the TiO_2 lattice from low levels in the Ti^{3+} d orbitals to the deep levels created by OH^- groups (acceptor behavior). As a result of the back-excitation of the TiO_2 lattice from low levels in the oxygen cavities to the ground state, two other peaks at 541 nm and 649 nm are formed (Figure 4(a)). The oxygen vacancies and surface hydroxyl groups are prevailing sites for trapped electrons and holes, respectively, due to vapor-thermal method used to synthesize TiO_2.

The PL spectra of FT with different %wt. Pt (%wt. 0, 0.5, 1, 2.5, and 5) are indicated in Figure 4(c). TiO_2 (T) showed a broad and more intense PL band than the FT and Pt doped FT samples due to the fast e^-/h^+ recombination rate. Due to the existence of Fe_3O_4 in FT, a decrease in UV emission peak located at 560 nm,[47] and a sharp red visible emission peak centered at 655 nm was detected for FT photocatalyst. PL intensity was substantially decreased by increasing %wt. Pt in the FT samples. This reveals that Pt plays an essential role to hinder the recombination of e^-/h^+ pairs.

The existence of broadband around 400–600 nm verified the recombination of the e^-/h^+ pairs because of the existence of the surface states and the self-trapped excites in the TiO_2.[48] The presence of Pt on the surface of FT indicated a decrease in the PL intensity of the photocatalyst, pointing out the rapid electron transfers from the conduction band (CB) of TiO_2 to Pt. Besides, the secondary peak between 600–650 nm is proof of the presence of oxygen vacancies in the related phase.[47]

The binding energies of FT-5.0% Pt were analyzed by X-ray photon spectroscopy (XPS) before and after the hydrogen production reaction. In Figure 5, Ti, Fe, O, and Pt elements can be distinguishable in the photocatalyst. The anatase TiO_2 shows conventional bands at 457.8 eV and 463.3 corresponding to the $Ti2p_{3/2}$ and $Ti2p_{1/2}$ spin-orbital splitting photoelectrons, respectively.[49] and it shows the presence of Ti^{4+}[15] as seen in Figure 5(a). After the hydrogen production reaction, bands shifted the binding energies of 458.7 and 464.0 eV for $Ti2p_{3/2}$ and $Ti2p_{1/2}$ corresponding to Ti^{4+}, respectively. (Figure 5 (a)). Thus, the red shift of the binding energy is probably related to Pt doping to the FT photocatalyst showing a decrease in the electron density of TiO_2 connecting with Pt.[50] It is proved that the electron charge density of Ti atoms and the bonding between Ti and O atoms was altered by the displacement of Pt ions.[26]

The O1s spectrum showed a lattice structure centered at 529 eV (Figure 5(c)), which corresponds to the lattice oxygen with high intensity, and the binding peak at 531.4 was attributed to the presence of surface oxygen, which represents

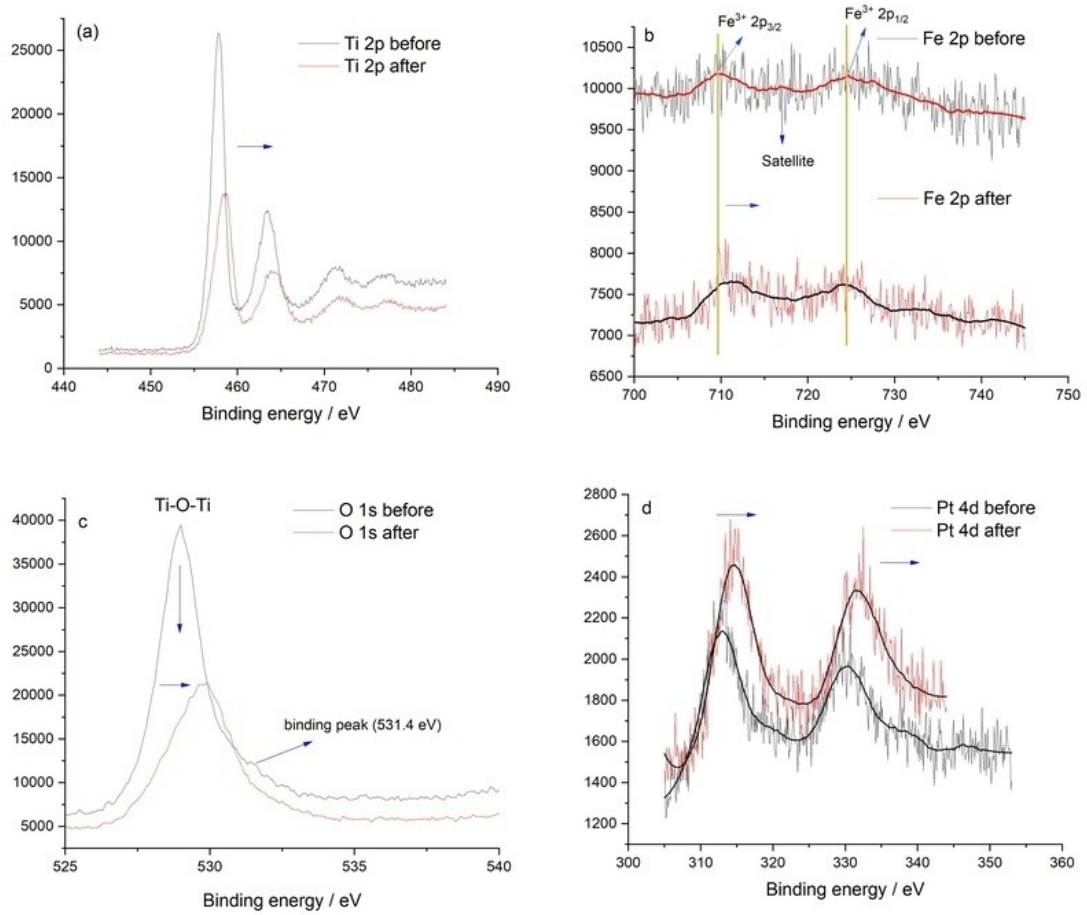

Figure 5. The XPS spectra of Ti2p (a), Fe2p (b), O1s (c), and Pt4d (d) in the photocatalyst before and after the hydrogen production reaction.

the lattice oxygen combined with Fe^{3+} and Ti^{4+}.[51] Besides, the weak peak at 530 eV was attributed to the defect oxygen vacancies (–OH) after the hydrogen production reaction.[37] The red shift of the peaks confirms the formation of substitution between TiO_2 and Fe due to the electronic interaction.[52] The decreasing intensity indicated a low oxygen vacancies/lattice oxygen ratio which means a low recombination rate.[53] The variation in the binding energy of Ti $2p_{3/2}$ and O 1s showed the existence of Ti–O–Pt bonds in FT sample.

The binding energies of 709.8 eV and 725.1 eV which are attributed to $Fe2p_{3/2}$ and $Fe2p_{1/2}$ in the photocatalyst were nearly the same in the literature (710.0 and 724.0 eV for Fe_3O_4), respectively[15,18] which indicates the characteristics of the mixed phase of Fe (II) and Fe (III), verifying the formation of Fe_3O_4 phase (Figure 5(b).[18] The satellite peak at 718.2 eV (Fe^{3+} $2p_{3/2}$) was proved mostly to be the Fe^{2+} ion state in Fe_3O_4 before the reaction.[43] However, the Fe $2p_{3/2}$ band shifted to a little bit higher energy as 711.1 eV and the $Fe2p_{1/2}$ band is nearly the same as 725 eV after the hydrogen production reaction, indicating that Fe^{2+} ions converted to Fe^{3+}on the surface of the photocatalyst by trapping the h^+. When the surface Fe^{2+}/Fe^{3+} molar ratio is low, it indicates that the surface has a low ratio of oxygen vacancies/lattice oxygen on the surface of the photocatalyst, which causes a low recombination rate.[53] Thus, the Fe^{2+}/Fe^{3+}ratio is getting lower after the reaction which causes a low recombination rate.

Pt 4d spectra showed binding energy of 313.1 eV and 330.5 eV for the metallic Pt corresponding to $4d_{5/2}$ and $4d_{3/2}$, respectively before the reaction. According to the literature, the binding energy for PtO is 317.3 eV and 314.6 eV for the metallic Pt at the surface which confirms the presence of metallic Pt species at the surface of the photocatalyst.[54] After the reaction, bands were nearly the same binding energies of 314.6 and 331.3 eV for Pt $4d_{5/2}$ and Pt $4d_{3/2}$, respectively. Consequently, these observations from XPS spectra essentially give insights that the synthesized FT–Pt photocatalyst contains the elements in $Ti^{3+/4+}$, $Fe^{2+/3+}$, and metallic Pt nanoparticles.

Photocatalytic activity measurement

Figure 6 shows the hydrogen production results for FT and FT–Pt photocatalysts with different wt.% of Pt. The hydrogen production increased in the order of FT-5.0 % Pt > FT-2.5 % Pt > FT-10 % Pt > FT-1.0 % Pt > FT-0.5 % Pt > FT after 5 h of photocatalytic reaction.

FT-5.0 wt.% Pt showed the highest amount of H_2 as 144 μmol/g-cat among all the photocatalysts. Enhanced photocatalytic activity of FT-5 wt.% Pt was attributed to the following factors as illustrated in Figure 7, i) 5 wt.% of Pt doping on the FT provided a suitable band gap, ii) Pt plays a vital role by trapping electrons to decrease e^-/h^+ recombination rate, iii) Fe^{2+} ions converted to Fe^{3+}on the surface of the photocatalyst by trapping the h^+ in the presence of Fe_3O_4 that make charge separation more facile.[55] In the literature, the H_2 production via Ag plasmons-sensitized magnetic-Fe_3O_4 integrated TiO_2 (Ag–Fe_3O_4@TiO_2) ternary nanocomposites was 911 μmol/g.h

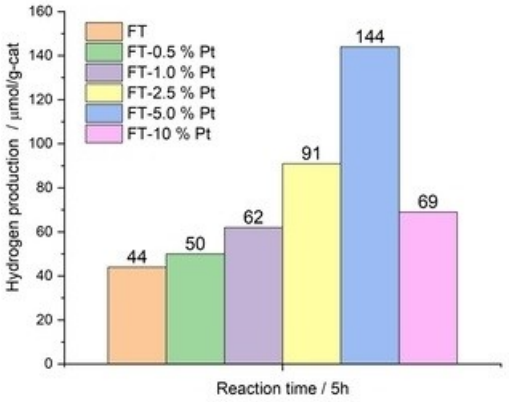

Figure 6. H_2 production over FT and FT–Pt photocatalysts with different wt.% of Pt.

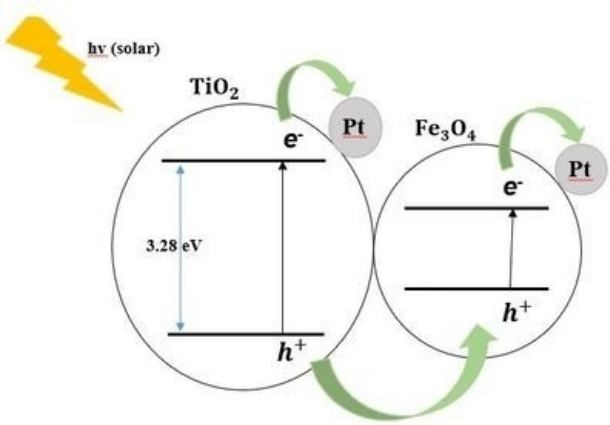

Figure 7. Proposed e^-/h^+ charge separation mechanism for FT-5.0 %Pt photocatalyst.

under light conditions as seen in Table 2. However, this article used higher amounts of Ag particles (noble metal like Pt in our study) in their study which is the most probable reason for the high H_2 production rate.[28] Another study that uses Fe_3O_4 and Co_3O_4 doped TiO_2 indicated that Fe and Co ions together improved solar light absorption of TiO_2, inhibited the recombination of photogenerated charges, and enhanced the photocatalytic activity of hydrogen production. They didn't observe H_2 in the case of pure TiO_2 while the 5% Fe_3O_4/TiO_2 gave a small amount of H_2 (~125 μmol/g) compared with 5% Fe_3O_4/Co_3O_4–TiO_2 after 5 h as seen in Table 2.[29]

Table 2. Comparison of H_2 production rate for different Fe_3O_4/TiO_2 catalysts.

Catalyst	H_2 production rate (μmol/g)	References
Fe_3O_4@TiO_2	335 (1 h)	[28]
Ag–Fe_3O_4@TiO_2	911(1 h)	[28]
5% Fe_3O_4/TiO_2	125 (5 h)	[29]
Pt doped Fe_3O_4–TiO_2 (FT-5.0 % Pt)	144 (5 h)	This work

To the best of our knowledge, Fe_3O_4–TiO_2 is a type I heterojunction which is not favorable for photocatalytic applications in terms of causing a higher e-/h + recombination rate.[32] In this type of photocatalyst, the photogenerated carriers would transfer across the heterojunction interface and accumulate on the Fe_3O_4 semiconductor and may act as an electron-hole recombination center.[34]

In Fe_3O4–TiO_2 heterojunctions (type I), the photogenerated electrons and holes of TiO_2 transferred to Fe_3O_4 more easily which makes a higher rate of recombination.[25] However, Pt doping on the TiO_2 surface plays a vital role as an electron acceptor to decrease the e^-/h^+ recombination rate and thus the enhanced photocatalytic activity was obtained with FT-5.0 wt.% Pt.

Conclusions

This work demonstrates the synthesis of solar light-driven Pt doped Fe_3O_4–TiO_2 photocatalysts and their usage of them in hydrogen production.

The results show that; the sensitivity of the catalyst to visible light radiation slightly increased when wt.% of Pt in the photocatalyst increased; FT photocatalyst has 3.25 eV band gap energy whereas FT-% 5.0 Pt has 2.95 eV bandgap energy; PL intensity was decreased by doping Pt to FT photocatalyst which indicates the retarded e^-/h^+ recombination; XPS spectra showed that Pt acts as an electron trapper; Fe^{2+}/Fe^{3+} ratio is getting lower after the hydrogen production reaction indicating that Fe_3O_4 acts as a hole acceptor. Besides, the red shift of the peaks in the O1s spectrum is confirming the formation of substitution between TiO_2 and Fe due to the electronic interaction after the hydrogen production reaction.

Consequently, FT-% 5.0 Pt can be proposed as a solar-light driven photocatalyst due to the highest amount of H_2 production rate as 144 μmol/g-cat. In this study the synergistic effect of Pt and Fe_3O_4 is found to be beneficial to decrease e^-/h^+ recombination rate thus the photocatalytic activity enhancement was achieved.

Supporting Information Summary

Detailed information about experimental methods and instruments for characterization used in the study conducted and additional figures are given in the supplementary information (SI).

Acknowledgements

This work was supported by TUBITAK (The Scientific and Technological Research Council of Turkey) with project number 216M386.

Conflict of Interests

The authors declare no conflict of interest.

Data Availability Statement

The data that support the findings of this study are available from the corresponding author upon reasonable request.

Keywords: Fe_3O_4–TiO_2 · Hydrogen (H_2) production · Photocatalysis

[1] P. Laokul, V. Amornkitbamrung, S. Seraphin, S. Maensiri, *Curr. Appl. Phys.* **2011**, *11(1)*, 101–108.
[2] Ö. Kerkez-Kuyumcu, E. Kibar, K. Dayıoğlu, F. Gedik, A. N. Akın, Ş. Özkara-Aydınoğlu, *J. Photochem. Photobiol. A* **2015**, *311*, 176–185.
[3] X. Zhu, F. Zhang, M. Wang, J. Ding, S. Sun, J. Bao, C. Gao, *Appl. Surf. Sci.* **2014**, *319*, 83–89.
[4] D. Komaraiah, E. Radha, J. Sivakumar, M. V. R. Reddy, R. Sayanna, *Opt. Mater.* **2020**, *108(1–14)*, 110401.
[5] B. Liu, X. Wang, G. Cai, L. Wen, Y. Song, X. Zhao, *J. Hazard. Mater.* **2009**, *169(1–3)*, 1112–1118.
[6] Y. Wang, C. Feng, Z. Jin, J. Zhang, J. Yang, S. Zhang, *J. Mol. Catal. A* **2006**, *260*, 1–3.
[7] S. Wang, S. Zhou, *J. Hazard. Mater.* **2011**, *185*, 77–85.
[8] J. Yan, L. Zhang, H. Yang, Y. Tang, Z. Lu, S. Guo, Y. Dai, Y. Han, M. Yao, *Sol. Energy* **2009**, *83*, 1534–1539.
[9] R. Liu, H. Yoshida, S. Fujita, M. Arai, *Appl. Catal. B* **2014**, *144*, 41–45.
[10] J. Shi, X. Yan, H.-J. Cui, X. Zong, M.-L. Fu, S. Chen, L. Wang, *J. Mol. Catal. A* **2012**, *356*, 53–60.
[11] Y. Wang, X. Meng, Q. Hu, M. Zhang, X. Cao, C. Xu, Y. Ding, *Int. J. Hydrogen Energy* **2021**, *46*, 6262–6271.
[12] J. Xu, Y. Ao, D. Fu, *Appl. Surf. Sci.* **2009**, *256*, 884–888.
[13] X. Yang, C. Cao, L. Erickson, K. Hohn, R. Maghirang, K. Klabunde, *Appl. Catal. B* **2009**, *91*, 657–662.
[14] A. K. L. Sajjad, S. Shamaila, B. Tian, F. Chen, J. Zhang, *J. Hazard. Mater.* **2010**, *177*, 781–791.
[15] H. S. Kim, D. Kim, B. S. Kwak, G. B. Han, M. H. Um, M. Kang, *Chem. Eng. J.* **2014**, *243*, 272–279.
[16] X. N. Wei, H. L. Wang, *J. Alloys Compd.* **2018**, *763*, 844–853.
[17] X. Zhao, R. Wang, Z. Lu, W. Wang, Y. Yan, *J. Photochem. Photobiol. A* **2019**, *382(1–10)*, 111902.
[18] H. Fan, G. Yi, X. Zhang, B. Xing, C. Zhang, L. Chen, Y. Zhang, *Opt. Mater.* **2021**, *111(1–10)*, 110582.
[19] M. Rafieezadeh, A. H. Kianfar, *J. Photochem. Photobiol. A* **2022**, *423(1–13)*, 113596.
[20] S. Narzary, K. Alamelu, V. Raja, B. M. Jaffar Ali, *J. Environ. Chem. Eng.* **2020**, *8(1–9)*, 104373.
[21] A. C. Chu, R. S. Sahu, T. S. Chou, Y. Shih, *J. Environ. Chem. Eng.* **2021**, *9(1–9)*, 105539.
[22] A. Sheikhmohammadi, E. Asgari, H. Nourmoradi, M. M. Fazli, M. Yeganeh, *J. Environ. Chem. Eng.* **2021**, *9(1–14)*, 105844.
[23] J. Ma, S. Guo, X. Guo, H. Ge, *Appl. Surf. Sci.* **2015**, *353*, 1117–1125.
[24] L. Zhang, Z. Wu, L. Chen, L. Zhang, X. Li, H. Xu, H. Wang, G. Zhu, *Solid State Sci.* **2016**, *52*, 42–48.
[25] X. Jia, R. Dai, D. Lian, S. Han, X. Wu, H. Song, *Appl. Surf. Sci.* **2017**, *392*, 268–276.
[26] Q. Zhang, L. Yu, B. Yang, C. Xu, W. Zhang, Q. Xu, G. Diao, *Chem. Phys. Lett.* **2021**, *774(1–9)*, 138609.
[27] X. An, D. Cheng, L. Dai, B. Wang, H. J. Ocampo, J. Nasrallah, X. Jia, J. Zou, Y. Long, Y. Ni, *Appl. Catal. B* **2017**, *206*, 53–64.
[28] M. P. Ravikumar, S. Bharathkumar, B. Urupalli, M. K. Murikinati, S. M. Venkatakrishnan, S. Mohan, *Energy Fuels* **2022**, *36(19)*, 11503–11514.
[29] M. M. Abutalib, H. M. Alghamdi, A. Rajeh, O. Nur c, A. M. Hezma, M. A. Mannaa, *J. Mater. Res. Technol.* **2022**, *20*, 1043–1056.
[30] I. Firtina-Ertis, Ö. Kerkez-Kuyumcu, *J. Photochem. Photobiol. A* **2022**, *432(1—11)*, 114106.
[31] S. Bakardjieva, J. Subrt, V. Stengl, M. J. Dianez, M. J. Sayagues, *Appl. Catal. B* **2005**, *58*, 193–202.

[32] S. Kumar, A. Kumar, A. Kumar, V. Krishnan, *Catal. Rev.* **2020**, *62(3)*, 346–405.
[33] V. M. Vinosel, S. Anand, M. A. Janifer, S. Pauline, S. Dhanavel, P. Praveena, A. Stephen, *Appl. Phys. A* **2019**, *125(1–13)*,319.
[34] J. López, A. Rey, E. Viñuelas-Zahinos, P. M. Álvarez, *J. Environ. Chem. Eng.* **2023**, *11*, 109999.
[35] N. Madima, K. K. Kefeni, A. T. Kuvarega, S. B. Mishra, A. K. Mishra, *Inorg. Chem. Commun.* **2022**, *145*, 109966.
[36] W. Bootluck, T. Chittrakarn, K. Techato, W. Khongnakorn, *J. Environ. Chem. Eng.* **2021**, *9(1–11)*, 105660.
[37] A. N. Chishti, Z. Ma, Y. Liu, M. Chen, J. Gautam, F. Guo, L. Ni, G. Diao, *Colloids Surf. A* **2021**, *631(1–13)*, 127694.
[38] R. M. Mohamed, M. W. Kadi, A. A. Ismail, *Ceram. Int.* **2020**, *46*, 15604–15612.
[39] L. Zhang, Z. Wu, L. Chen, L. Zhang, X. Li, H. Xu, H. Wang, G. Zhu, *Solid State Sci.* **2016**, *52*, 42–48.
[40] W. Septina, S. Ikeda, M. A. Khan, T. Hirai, T. Harada, M. Matsumura, L. M. Peter, *Electrochim. Acta* **2011**, *56*, 4882–4888.
[41] N. Singh, R. M. Mehra, A. Kapoor, *J. Nano – Electron. Phys.* **2011**, *3*, 132–139.
[42] M. Stefan, O. Pana, C. Leostean, C. Bele, D. Silipas, M. Senila, E. Gautron, *J. Appl. Phys.* **2014**, *116*, 114312.
[43] R. Hatefi, H. Younesi, A. Mashinchian-Moradi, S. Nojavan, *Adv. Powder Technol.* **2021**, *32*, 2410–2422.
[44] N. Kislov, S. S. Srinivasan, Y. Emirov, E. K. Stefanakos, *Mater. Sci. Eng. B* **2008**, *153*, 70–77.
[45] F. Yakuphanoğlu, *J. Alloys Compd.* **2010**, *507*, 184–189.
[46] L. Chetibi, T. Busko, N. P. Kulish, D. Hamana, S. Chaieb, S. Achour, *J. Nanopart. Res.* **2017**, *19(1–9)*, 129.
[47] S. Khashan, S. Dagher, N. Tit, A. Alazzam, I. Obaidat, *Surf. Coat. Technol.* **2017**, *322*, 92–98.
[48] R. Bashiri, N. M. Mohamed, L. Y. Ling, N. A. Suhaimi, M. U. Shahid, S. Sufian, C. F. Kait, S. M. Saheed, *Diamond Relat. Mater.* **2019**, *94*, 194–202.
[49] L. Ge, M. Xu, H. Fang, M. Sun, *Appl. Surf. Sci.* **2006**, *253(2)*, 720–725.
[50] H. S. Ferreira, H. S. Ferreira, M. V. S. da Silva, M. G. C. da Rocha, P. Bargiela, M. C. Rangel, K. I. B. Eguiluz, G. R. Salazar-Banda, *Mater. Chem. Phys.* **2020**, *245(1–10)*, 122753.
[51] R. Huang, R. Liang, H. Fan, S. Ying, L. Wu, X. Wang, G. Yan, *Sci. Rep.* **2017**, *7(1–10)*, 7858.
[52] O. Ibukun, H. K. Jeong, *Chem. Phys. Lett.* **2019**, *730*, 259–265.
[53] R. Bashiri, M. F. R. Samsudin, N. M. Mohamed, N. A. Suhaimi, L. Y. Ling, S. Sufian, C. F. Kait, *Appl. Surf. Sci.* **2020**, *510(1–10)*, 145482.
[54] N. S. Resende, C. A. Perez, J. G. Eon, M. Schmal, *Catal. Lett.* **2011**, *141*, 1685–1692.
[55] P. A. K. Reddy, S. Basavaraju, D. K. Valluri, V. S. Muthukonda, S. Machiraju, J. S. Lee, *Chem. Eng. J.* **2014**, *247*, 152–160.

Manuscript received: March 31, 2023